

A spectroscopic study of the Globular Cluster M28 (NGC 6626)^{*}

S. Villanova^{1†}, C. Moni Bidin², F. Mauro¹, C. Munoz¹, and L. Monaco³

¹*Departamento de Astronomía, Casilla 160, Universidad de Concepción, Chile*

²*Instituto de Astronomía, Universidad Católica del Norte, Av. Angamos 0610 Antofagasta Chile*

³*Universidad Andres Bello, Departamento de Ciencias Físicas, Republica 220, Santiago, Chile*

Accepted –. Received –; in original form –

ABSTRACT

We present the abundance analysis for a sample of 17 red giant branch stars in the metal-poor globular cluster M28 based on high resolution spectra. This is the first extensive spectroscopic study of this cluster. We derive abundances of O, Na, Mg, Al, Si, Ca, Ti, V, Cr, Mn, Fe, Co, Ni, Cu, Zn, Y, Zr, Ba, La, Ce, and Eu. We find a metallicity of $[\text{Fe}/\text{H}] = -1.29 \pm 0.01$ and an α -enhancement of $+0.34 \pm 0.01$ (errors on the mean), typical of Halo Globular Clusters in this metallicity regime. A large spread is observed in the abundances of light elements O, Na, and Al. Mg also shows an anticorrelation with Al with a significance of 3σ . The cluster shows a Na-O anticorrelation and a Na-Al correlation. This correlation is not linear but “segmented” and that the stars are not distributed continuously, but form at least 3 well separated sub-populations. In this aspect M28 resembles NGC 2808 that was found to host at least 5 sub-populations. The presence of a Mg-Al anticorrelation favor massive AGB stars as the main polluters responsible for the multiple-population phenomenon.

Key words: Chemical Abundances – Globular Cluster: M28 (NGC 6626).

1 INTRODUCTION

Galactic Globular Clusters (GCs) are known to host star-to-star variations as far as chemical abundances are concerned. More specifically, Carretta et al. (2009b) showed that all Galactic GCs studied up to now have at least a spread (or anti-correlation) in the content of their light-elements O and Na. In some cases also a Mg and Al spread is observed. The only confirmed exception is Ruprecht 106, where Villanova et al. (2013) found that stars share a homogenous chemical composition. This spread is due to the early evolution of each cluster, that is initially formed by a first generation of stars that has the same chemical composition of field stars at the same metallicity. The subsequent generation of stars (Na-richer and O-poorer) are formed from gas polluted by ejecta of evolved stars of the older generation (Na-poorer and O-richer). This is the so called multiple-population phenomenon. These anomalies have also been observed in one of the old, massive extragalactic GCs in Fornax (Letarte et al. 2006; Larsen et al. 2012) and in the Large Magellanic Cloud (LMC; Mucciarelli et al. 2009), but not in intermediate-age LMC clusters (Mucciarelli et al. 2014). This spectroscopic evidence has been interpreted as the sig-

nature of material processed during H-burning by high temperature proton-capture reactions (such as the Ne-Na and Mg-Al cycles). Several theoretical models have been proposed to describe the formation and early evolution of GCs (e.g. D’Antona et al. 2016) The current explanation involves a self-enrichment scenario, were subsequent generations of stars co-exist in globular clusters that are formed from gas polluted by processed material produced by massive stars (Caloi & D’Antona 2011). Several sources of polluters have been proposed: intermediate-mass asymptotic giant branch (AGB) stars (D’Antona et al. 2016), fast-rotating massive stars (Decressin et al. 2007), and massive binaries (De Mink et al. 2009). All these scenarios postulate that an important fraction of the first generation has been lost in order to justify the relatively low fraction of these stars that are observed nowadays compared with the objects of the Na-richer and O-poorer generations. A recent attractive alternative has been proposed by Bastian et al. (2013) that implies only a single burst of star formation. They postulate that the gas ejected from massive stars of the first (and the only) generation concentrates in the center of the cluster and is acquired by low-mass stars via disk accretion, while they are in the fully convective phase of the pre-main sequence. This scenario has the advantage that does not require a huge star loss. However it is not able to reproduce the Mg-Al an-

† E-mail: svillanova@astro-udec.cl (SV)

ticorrelation that is observed in some GCs like NGC 2808 (D’Antona et al. 2016).

In addition to the abundance spread of light elements, variations in heavier elements have also been found in some massive GCs, such as ω Centauri (Villanova et al. 2014), M54 (Carretta et al. 2010), M22 (Marino et al. 2009), Terzan5 (Massari et al. 2014) and NGC 2419 (Cohen et al. 2010). However they are generally thought to be the vestige of more massive primitive dwarf galaxies that merged with the Galaxy.

In this paper we present a spectroscopic study of the GC M28 (NGC 6626). This is an old and metal-poor globular cluster that has received little attention, mostly due to reddening problems and the strong field contamination since it is located toward the Galactic Bulge slightly below the Galactic plane ($l=7.80^{\circ}$, $b=-5.58^{\circ}$). M28 has a low metallicity of $[\text{Fe}/\text{H}]=-1.32$ and a high reddening of $E(BV)=0.40$ (Harris 1996). The best photometry we could find in literature is that from Davidge et al. (1996) that shows a color-magnitude diagram (CMD) characteristic of metal-poor clusters with a horizontal branch (HB) that extends far to the blue. Its HB looks more like that of a very metal poor GCs such as NGC 6397 ($[\text{Fe}/\text{H}]=-2.0$) or NGC 7078 ($[\text{Fe}/\text{H}]=-2.3$) than that of a GC of the same metallicity such as NGC 1851 ($[\text{Fe}/\text{H}]=-1.2$) or NGC 288 ($[\text{Fe}/\text{H}]=-1.3$) because M28 lacks completely a red HB. From this we infer that M28 is significantly older than NGC 1851 or NGC 288 (11.0 and 11.5 Gyrs respectively, Vandenberg et al. 2013) with an age comparable to that of M12 ($[\text{Fe}/\text{H}]=-1.3$ and Age=13.0 Gyrs) based on the fact that also M12 completely lacks a red HB (D’Orazi et al. 2014). At only 2.7 kpc from the Galactic center (Harris 1996), M28 is one of the most metal-poor GCs found in the inner Galaxy, and it was classified as a genuine Bulge GCs by Bica et al. (2015). If it is really as old as M12, M28 could be one of the oldest Bulge objects.

In section 2 we describe observation and data reduction and in section 3 the methodology we used to obtain the chemical abundances and the associated errors. In section 4 we present our results including a comparison with different environments (Galactic and extragalactic). Finally in section 5 we give a summary of our findings.

2 OBSERVATIONS AND DATA REDUCTION

Our dataset consists of high resolution spectra collected at the FLAMES@UVES spectrograph mounted at the VLT-UT2 telescope. Targets were selected from the infrared photometry collected with the Vista Variables in the Via Lactea survey (VVV, Minniti et al. 2010; Saito et al. 2012). The PSF photometry was obtained with the VVV-SkZ_pipeline (Mauro et al. 2013) on the publicly available pre-processed frames, and calibrated in the astrometric and photometric 2MASS system (Skrutskie et al. 2001) as detailed in Moni Bidin et al. (2011) and Chene et al. (2012). A total of 17 stars were selected along the upper red giant cluster sequence with magnitude between $K_s=8.5$ and $K_s=11$. The position of the targets in the cluster VVV color-magnitude diagram (CMD) is shown in Fig 1. These stars were observed with four fiber configurations of FLAMES@UVES. We used the 580nm set-up, that gives a spectral coverage

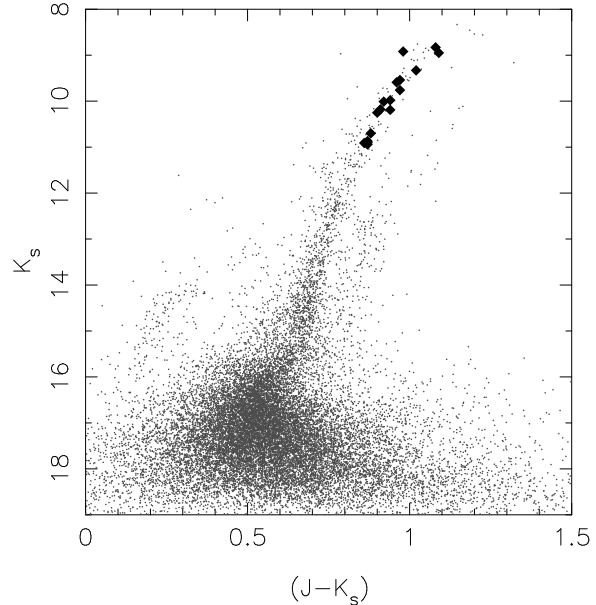


Figure 1. K_{2MASS} vs. $J-K_{2MASS}$ CMD of M28. Target stars are indicated as filled black circles.

between 4800 and 6800 Å with a resolution of $R=47000$. The signal-to-noise (S/N) was between 50 and 70 at 6000 Å. Four targets were observed twice, in two different fiber configurations, to perform a proper error analysis.

Data were reduced using the dedicated pipeline¹. Data reduction includes bias subtraction, flat-field correction, wavelength calibration, sky subtraction, and spectral rectification.

Radial velocities were measured by the *fixcor* package in IRAF², using a synthetic spectrum as a template. The mean radial velocity we obtained is 13.3 ± 2.0 km/s. Harris (1996) gives 17 ± 1 instead. The agreement is good if we consider that the cluster has a large velocity dispersion as shown by the R.M.S. of our stars that is 9.4 ± 1.5 km/s. There are not clear outliers in the radial velocity distribution. If we consider also that all our targets have the same $[\text{Fe}/\text{H}]$ content within errors (see Section 4) and that all lie along the Red Giant sequence in the cluster CMD, we conclude that they are all cluster member. Table 1 lists the basic parameters of the retained stars: ID (stars observed twice are indicated by an underscored number), 2MASS ID, J2000.0 coordinates (RA & DEC in degrees), VVV J, H, K_s magnitudes, heliocentric radial velocity RV_H (km/s), T_{eff} (K), $\log(g)$, micro-turbulence velocity v_t (km/s), and $[\text{Fe}/\text{H}]$ abundances. The determination of the atmospheric parameters and abundances is discussed in the next section. In this table we report also the cluster mean radial velocity and mean $[\text{Fe}/\text{H}]$ abundance with their errors (errors on the mean). In Fig. 1 we report, on the top of the M28 color magnitude diagram (CMD), our targets as black filled points. We warn the reader that the four targets observed twice have

¹ see <http://www.eso.org/sci/software/pipelines/>

² IRAF is distributed by the National Optical Astronomy Observatory, which is operated by the Association of Universities for Research in Astronomy, Inc., under cooperative agreement with the National Science Foundation.

Table 1. ID numbers, coordinates, VVV (J,H,K) magnitudes, heliocentric radial velocities and atmospheric parameters for the observed stars. Reported errors are errors on the mean.

ID	ID(2MASS)	RA degree s	DEC degrees	J mag.	H mag.	K mag.	RV _H km/s	T _{eff} K	log(g) dex	v _t km/s	[Fe/H] dex
1236	18242731-2452349	276.113810	-24.876362	11.811	11.129	10.944	2.6	4617	1.80	1.40	-1.16
1239	18242792-2451160	276.116356	-24.854464	11.748	11.045	10.874	0.0	4537	1.56	1.32	-1.20
1246 ₁	18242914-2452024	276.121430	-24.867336	10.935	10.197	10.014	18.8	4218	0.94	1.39	-1.30
1246 ₂	18242914-2452024	276.121430	-24.867336	10.935	10.197	10.014	19.9	4252	1.00	1.42	-1.32
1280	18243130-2452471	276.130424	-24.879751	10.722	9.969	9.756	18.0	4219	0.99	1.49	-1.38
1282	18243140-2451136	276.130842	-24.853786	10.042	9.125	8.951	8.8	3983	0.44	1.56	-1.38
1291	18243191-2453293	276.132983	-24.891479	10.351	9.533	9.335	7.0	4091	0.64	1.48	-1.32
1293 ₁	18243208-2452567	276.133679	-24.882437	9.910	9.053	8.827	26.8	3945	0.49	1.55	-1.38
1293 ₂	18243208-2452567	276.133679	-24.882437	9.910	9.053	8.827	28.0	3974	0.53	1.54	-1.34
1295	18243227-2452471	276.134463	-24.879768	10.510	9.746	9.545	12.6	4180	0.84	1.47	-1.32
1315	18243318-2451079	276.138277	-24.852196	11.125	10.372	10.186	1.0	4297	1.04	1.43	-1.27
1328	18243398-2451227	276.141588	-24.856312	10.924	10.181	9.983	11.8	4301	1.14	1.42	-1.23
1330	18243399-2450583	276.141626	-24.849554	11.581	10.864	10.701	15.1	4426	1.27	1.28	-1.28
1343	18243460-2452406	276.144202	-24.877949	11.774	11.095	10.905	24.7	4571	1.68	1.35	-1.20
1364	18243590-2452090	276.149619	-24.869192	11.768	11.089	10.910	8.9	4508	1.46	1.36	-1.30
1367	18243627-2452221	276.151166	-24.872833	11.086	10.339	10.178	19.3	4323	1.22	1.40	-1.34
1378 ₁	18243700-2451179	276.154185	-24.854994	10.551	9.763	9.587	-2.0	4161	0.85	1.48	-1.26
1378 ₂	18243700-2451179	276.154185	-24.854994	10.551	9.763	9.587	-1.4	4107	0.64	1.42	-1.32
1380 ₁	18243713-2452257	276.154724	-24.873831	9.900	9.040	8.919	18.6	4098	0.80	1.53	-1.24
1380 ₂	18243713-2452257	276.154724	-24.873831	9.900	9.040	8.919	19.4	4052	0.54	1.46	-1.28
1402	18243900-2451077	276.162541	-24.852152	11.146	10.397	10.246	20.3	4391	1.32	1.46	-1.27
Cluster							13.3				-1.29
Error							2.0				0.01

Table 2. Chemical abundances of our stars (Part 1). The abundance for Ti is the mean of those obtained from the neutral and singly ionized species. Reported errors are errors on the mean.

ID	[OI/Fe]	[NaI/Fe]	[MgI/Fe]	[AlII/Fe]	[SiII/Fe]	[CaI/Fe]	[Ti/Fe]	[VI/Fe]	[CrI/Fe]	[MnI/Fe]
1236	-0.58	0.41	0.43	1.01	0.28	0.39	0.36	0.45	0.02	-0.47
1239	-0.51	0.44	0.50	1.06	0.32	0.31	0.30	0.24	-0.01	-0.42
1246 ₁	0.05	0.43	0.46	0.48	0.35	0.33	0.34	0.34	-0.03	-0.49
1246 ₂	-0.08	0.39	0.55	0.46	0.31	0.35	0.31	0.27	-0.09	-0.39
1280	0.35	-0.06	0.52	0.30	0.34	0.41	0.34	0.35	0.07	-0.34
1282	0.29	0.00	0.49	0.17	0.35	0.40	0.30	0.33	-0.04	-0.36
1291	-0.72	0.58	0.44	1.07	0.37	0.39	0.29	0.35	0.03	-0.34
1293 ₁	0.23	-0.05	0.44	0.24	0.38	0.35	0.26	0.29	0.07	-0.39
1293 ₂	0.32	-0.02	0.46	0.20	0.31	0.35	0.29	0.42	-0.05	-0.37
1295	-0.79	0.72	0.44	1.02	0.37	0.40	0.31	0.35	0.00	-0.35
1315	-0.17	0.38	0.43	0.73	0.40	0.42	0.32	0.31	0.04	-0.39
1328	-0.61	0.46	0.36	1.10	0.38	0.36	0.32	0.33	-0.01	-0.40
1330	-0.55	0.54	0.45	1.05	0.43	0.42	0.36	0.22	-0.08	-0.38
1343	0.17	0.17	0.51	0.32	0.24	0.30	0.33	0.43	0.04	-0.42
1364	-0.46	0.44	0.49	0.93	0.31	0.40	0.36	0.29	-0.03	-0.35
1367	-0.04	0.42	0.50	0.42	0.40	0.40	0.34	0.28	-0.19	-0.39
1378 ₁	0.28	-0.07	0.45	0.11	0.28	0.39	0.32	0.37	-0.10	-0.33
1378 ₂	0.20	0.02	0.53	0.15	0.34	0.38	0.28	0.21	-0.08	-0.39
1380 ₁	0.30	-0.10	0.50	0.22	0.23	0.36	0.31	0.44	-0.02	-0.34
1380 ₂	0.20	-0.04	0.49	0.16	0.33	0.35	0.27	0.37	0.00	-0.37
1402	-0.44	0.55	0.47	1.03	0.33	0.37	0.34	0.44	-0.02	-0.36
Cluster	-0.12	0.27	0.47	0.58	0.34	0.37	0.32	0.34	-0.02	-0.38
Error	0.09	0.06	0.01	0.08	0.01	0.01	0.01	0.02	0.01	0.01

Table 3. Chemical abundances of our stars (Part 2). Reported errors are errors on the mean.

ID	[CoI/Fe]	[NiII/Fe]	[CuI/Fe]	[ZnI/Fe]	[YII/Fe]	[ZrII/Fe]	[BaII/Fe]	[LaII/Fe]	[CeII/Fe]	[EuII/Fe]
1236	0.13	-0.02	-	0.09	0.12	0.25	0.35	-0.33	0.12	0.39
1239	0.14	-0.01	-0.29	0.19	0.09	0.30	0.34	-0.18	-0.05	0.41
1246 ₁	0.04	0.02	-	-	-	0.12	-	-	-	0.53
1246 ₂	0.09	-0.04	-0.17	-	0.17	0.24	0.35	-0.07	-0.01	0.47
1280	0.11	-0.04	-0.25	0.23	0.16	0.34	0.24	0.13	-0.33	0.40
1282	0.10	-0.05	-0.20	-	0.16	0.29	0.20	0.06	-0.28	0.32
1291	0.11	-0.03	-0.25	0.32	0.24	0.27	0.44	0.14	-0.13	0.36
1293 ₁	0.08	0.00	-0.11	-0.04	0.07	0.26	0.20	-	-0.07	0.39
1293 ₂	0.08	-0.03	-0.14	0.02	0.07	0.26	0.35	0.03	-0.19	0.37
1295	0.10	-0.05	-0.24	0.26	0.27	0.26	0.41	-0.06	-0.14	0.36
1315	0.08	-0.07	-0.17	0.21	0.14	0.23	0.22	-0.36	-0.11	0.37
1328	0.08	-0.06	-0.34	0.31	0.21	0.22	0.27	-0.09	-0.21	0.13
1330	-0.07	-0.03	-0.25	0.26	0.14	0.25	0.25	-0.25	-0.27	0.28
1343	0.08	-0.01	-	-	0.01	0.26	0.20	0.01	-0.19	0.29
1364	0.12	-0.01	-	0.20	0.12	0.26	0.30	0.07	-0.39	0.31
1367	0.03	0.03	-0.29	0.04	0.22	0.28	0.23	0.17	-0.15	0.46
1378 ₁	0.15	-0.04	-0.25	0.13	-	0.22	0.34	-	-0.26	0.35
1378 ₂	0.09	-0.10	-0.22	0.35	0.11	0.24	0.26	-0.15	-0.27	0.24
1380 ₁	0.05	-0.03	-0.27	0.09	0.13	0.32	0.34	0.06	-0.04	0.36
1380 ₂	0.08	-0.05	-0.19	0.23	0.15	0.25	0.36	0.02	-0.20	0.35
1402	0.09	-0.03	-0.13	0.11	0.15	0.30	0.38	0.18	-0.23	0.26
Cluster	0.08	-0.03	-0.22	0.18	0.14	0.26	0.30	-0.03	-0.17	0.35
Error	0.01	0.01	0.02	0.03	0.01	0.01	0.02	0.04	0.03	0.02

Table 4. Estimated errors on abundances due to errors on atmospheric parameters and to spectral noise for star #1367 (column 2 to 6). Column 7 gives the total error calculated as the root squared of the sum of the squared of columns 2 to 6. This total error must be compared with the total error as obtained from the 4 repeated stars (column 8) and with the observed dispersion (RMS) of the data with its error (column 9). The last column gives the significance of the difference between the total error for star #1367 and the observed dispersion, in units of σ .

ID	$\Delta T_{\text{eff}}=40$ K	$\Delta \log(g)=0.12$	$\Delta v_t=0.04$ km/s	$\Delta [\text{Fe}/\text{H}]=0.03$	S/N	Δ_{tot}	$\Delta_{\text{tot}}(\text{obs})$	RMS_{obs}	Significance (σ)
$\Delta([\text{O}/\text{Fe}])$	0.02	0.06	0.01	0.01	0.05	0.08	0.07	0.40±0.06	5.3
$\Delta([\text{Na}/\text{Fe}])$	0.02	0.02	0.01	0.00	0.03	0.04	0.04	0.27±0.06	3.8
$\Delta([\text{Mg}/\text{Fe}])$	0.01	0.01	0.01	0.00	0.03	0.04	0.03	0.04±0.01	0.0
$\Delta([\text{Al}/\text{Fe}])$	0.01	0.02	0.01	0.01	0.04	0.05	0.03	0.39±0.06	5.7
$\Delta([\text{Si}/\text{Fe}])$	0.03	0.02	0.01	0.01	0.03	0.05	0.06	0.05±0.01	0.0
$\Delta([\text{Ca}/\text{Fe}])$	0.02	0.02	0.00	0.01	0.04	0.05	0.01	0.04±0.01	1.0
$\Delta([\text{Ti}/\text{Fe}])$	0.03	0.02	0.00	0.01	0.03	0.05	0.02	0.03±0.01	2.0
$\Delta([\text{V}/\text{Fe}])$	0.04	0.02	0.00	0.01	0.05	0.07	0.09	0.07±0.01	0.0
$\Delta([\text{Cr}/\text{Fe}])$	0.03	0.02	0.00	0.01	0.04	0.06	0.05	0.06±0.01	0.0
$\Delta([\text{Mn}/\text{Fe}])$	0.03	0.01	0.01	0.00	0.02	0.04	0.05	0.04±0.01	0.0
$\Delta([\text{Fe}/\text{H}])$	0.05	0.02	0.01	0.01	0.01	0.06	0.03	0.06±0.01	0.0
$\Delta([\text{Co}/\text{Fe}])$	0.02	0.01	0.01	0.00	0.06	0.07	0.03	0.05±0.01	2.0
$\Delta([\text{Ni}/\text{Fe}])$	0.00	0.02	0.00	0.00	0.02	0.03	0.02	0.03±0.01	0.0
$\Delta([\text{Cu}/\text{Fe}])$	0.01	0.02	0.01	0.01	0.07	0.08	0.04	0.06±0.01	2.0
$\Delta([\text{Zn}/\text{Fe}])$	0.05	0.03	0.01	0.00	0.09	0.11	0.06	0.11±0.02	0.0
$\Delta([\text{Y}/\text{Fe}])$	0.03	0.05	0.01	0.01	0.03	0.08	0.01	0.06±0.01	2.0
$\Delta([\text{Zr}/\text{Fe}])$	0.03	0.04	0.01	0.01	0.03	0.06	0.06	0.04±0.01	2.0
$\Delta([\text{Ba}/\text{Fe}])$	0.03	0.02	0.03	0.00	0.03	0.06	0.08	0.07±0.01	1.0
$\Delta([\text{La}/\text{Fe}])$	0.02	0.06	0.00	0.01	0.08	0.10	-	0.16±0.03	2.0
$\Delta([\text{Ce}/\text{Fe}])$	0.03	0.05	0.01	0.01	0.06	0.09	0.06	0.12±0.02	1.5
$\Delta([\text{Eu}/\text{Fe}])$	0.03	0.05	0.01	0.01	0.05	0.08	0.03	0.09±0.01	1.0

two points for each plot of this paper. We preferred to keep the measurements (abundances and atmospheric parameters) of each of the two spectra per target separated both in the text, in the tables and in the plots in order to allow a direct check of the internal errors of our analysis. When

required the two measurements per stars will be indicated by different symbols in the plots and by the underscores 1 and 2 in the text and in the tables.

3 ABUNDANCE ANALYSIS

Initial atmospheric parameters were obtained in the following way. First, T_{eff} was derived from the J-K color using the relation of Ramirez & Melendez (2005). The reddening we adopted ($E(B-V)=0.40$) was obtained from Harris (1996, 2010 edition). Surface gravities ($\log(g)$) were obtained from the canonical equation:

$$\log\left(\frac{g}{g_{\odot}}\right) = \log\left(\frac{M}{M_{\odot}}\right) + 4\log\left(\frac{T_{\text{eff}}}{T_{\odot}}\right) - \log\left(\frac{L}{L_{\odot}}\right).$$

where the mass M was assumed to be $0.8 M_{\odot}$, and the luminosity L/L_{\odot} was obtained from the absolute magnitude M_V assuming an apparent distance modulus of $(m-M)_V=15.55$ (Harris 1996). The bolometric correction (BC) was derived by adopting the relation BC- T_{eff} from Alonso et al. (1999). Finally, micro-turbulence velocity (v_t) was obtained from the relation of Marino et al. (2008). Atmospheric models were calculated using ATLAS9 code (Kurucz 1970) assuming our estimations of T_{eff} , $\log(g)$, and v_t , and the $[\text{Fe}/\text{H}]$ value from Harris (1996) ($[\text{Fe}/\text{H}]=-1.32$).

Then T_{eff} , $\log(g)$, and v_t were re-adjusted and new atmospheric models calculated in an interactive way in order to remove trends in excitation potential and reduced equivalent width (EQW) versus abundance for T_{eff} and v_t , respectively, and to satisfy the ionization equilibrium for $\log(g)$. 140–150 FeI lines and 12–14 FeII lines (depending on the S/N of the spectrum) were used for the latter purpose. The $[\text{Fe}/\text{H}]$ value of the model was changed at each iteration according to the output of the abundance analysis. The Local Thermodynamic Equilibrium (LTE) program MOOG (Snedden 1973) was used for the abundance analysis.

SiI, CaI, TiI, TiII, CrI, FeI, FeII, and NiI abundances were estimated using the EQW method. For this purpose we measured EQW using the automatic program DAOSPEC (Stetson & Pancino 2008)³. OI, NaI, MgI, AlI, VI, MnI, CoI, CuI, ZnI, YII, ZrII, BaII, LaII, CeII, and EuII abundances were obtained using the spectro-synthesis method. For this purpose 5 synthetic spectra were generated for each line with 0.25 dex abundance step and compared with the observed spectrum. The line-list and the methodology we used are the same used in previous papers (e.g. Villanova et al. 2013), so we refer to those articles for a detailed discussion about this point. Here we just underline that we took hyperfine splitting into account for Ba as in our previous studies. This is particularly important because Ba lines are very strong even in metal-poor stars and hyperfine splitting help to remove the line-core saturation producing a change in the final abundance as estimated by the spectro-synthesis method up to 0.1 dex. Also other odd-elements like V, Mn, Co, Cu, Y, and Eu or elements that have odd-isotopes like La and Ce have an hyperfine splitting, but their lines are weak and the line-core saturation is not at work. So hyperfine splitting corrections are negligible.

We also added the MgI line at 5528 Å. Parameters for this line were taken from SPECTRUM v2.76⁴ linelist (Gray & Corbally 1994). The abundances we obtained are

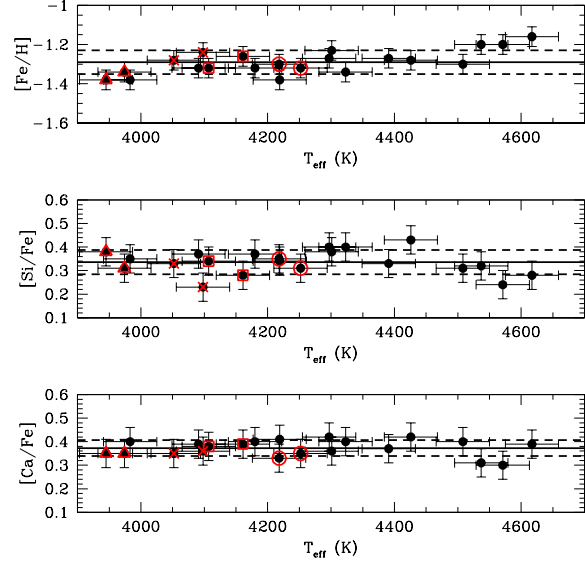


Figure 2. $[\text{Fe}/\text{H}]$, $[\text{Si}/\text{Fe}]$, and $[\text{Ca}/\text{Fe}]$ vs. T_{eff} for our targets. The 4 stars observed twice are indicated with 4 different red open symbols.

reported in Tab. 2 and Tab. 3 together with the mean values for the cluster and the error on the mean. For Ti we reported the mean values of TiI and TiII abundances. Na is an element affected by NLTE effects. For this reason we looked in the INSPEC⁵ database for suitable NLTE corrections. We found they are very small (~ 0.05 dex) with no significant variation (less than 0.02 dex) in our temperature range. For this reason we decided not to apply them to our Na abundances.

As a cross check of our abundance analysis, we plot in Fig. 2, Fig. 3, Fig. 4 and Fig. 5 $[\text{Fe}/\text{H}]$, $[\text{Si}/\text{Fe}]$, and $[\text{Ca}/\text{Fe}]$ vs. T_{eff} , $[\text{Ti}/\text{Fe}]$, $[\text{Ni}/\text{Fe}]$, and $[\text{Ba}/\text{Fe}]$ vs. T_{eff} , $[\text{O}/\text{Fe}]$ and $[\text{Na}/\text{Fe}]$ vs. T_{eff} , and $[\text{Mg}/\text{Fe}]$ and $[\text{Al}/\text{Fe}]$ vs. T_{eff} respectively, for the entire sample. The temperature range covered by our stars is about 600 K. We plot also the mean abundance for each element and the $\pm 1\sigma$ error.

$[\text{Fe}/\text{H}]$ shows a trend as a function of temperature with a significance on the slope of about 4σ , with warmer stars being more metal rich. In order to investigate this, first of all we plot in Fig. 6 (upper and middle panels) the line by line FeI and FeII differential abundances as a function of E.P. for stars #1236 and #1293₁. These stars were selected to be at the extremes of the T_{eff} range. Differential iron abundances were calculated by subtracting to each FeI and FeII line the average FeI abundance. FeI lines have a flat trend (the black continuous line) while FeII lines are spread around the mean FeI abundance. This is not surprising since Temperature and gravity were obtained in order to have flat trend for FeI lines and to match mean FeI and FeII abundances. However this test shows that the procedure was applied correctly. The $[\text{Fe}/\text{H}]$ trend could be due to departure from the LTE approximation we are using in our data analysis (the NLTE effect). In order to check this, for a subsample of 23 Fe I lines

³ DAOSPEC is freely distributed by <http://www.cadc-ccda.hia-ihp.nrc-cnrc.gc.ca/en/community/STETSON/daospec/>

⁴ <http://www.appstate.edu/~grayro/spectrum/spectrum.html>

⁵ version 1.0 (<http://inspect.coolstars19.com/index.php?n=Main.HomePage>)

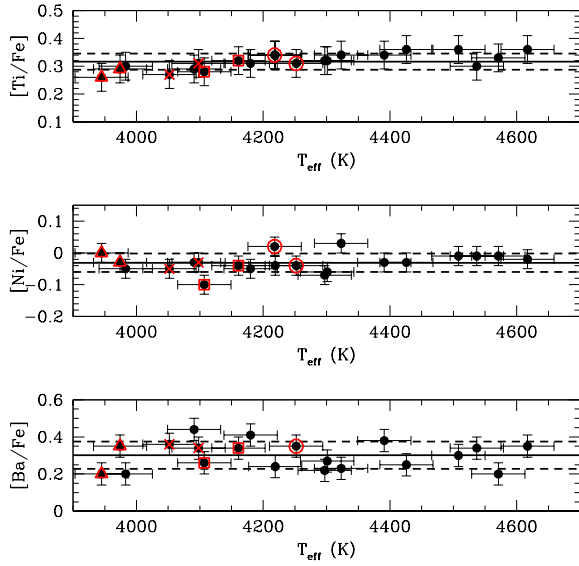


Figure 3. [Ti/Fe], [Ni/Fe], and [Ba/Fe] vs. T_{eff} for our targets. The 4 stars observed twice are indicated with 4 different red open symbols.

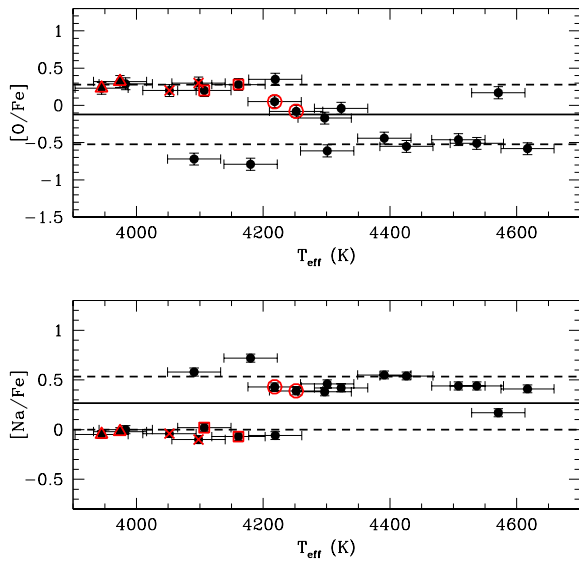


Figure 4. [O/Fe] and [Na/Fe] vs. T_{eff} for our targets. The 4 stars observed twice are indicated with 4 different red open symbols.

we obtained NLTE correction from the INSPEC⁶ database. The mean NLTE correction for #1236 is +0.06 while for #1293₁ id +0.01. This goes in the wrong direction, because the net effect would be to make the warmer stars even more metal rich compared with the cooler. However, as shown in Fig. 6 (lower panel), there is a trend of the NLTE correction with the exitation potential. This is not unexpected because lines with low E.P. form in the upper atmosphere where gas density is lower and detarture from LTE is larger.

⁶ version 1.0 (<http://inspect.coolstars19.com/index.php?n=Main.HomePage>)

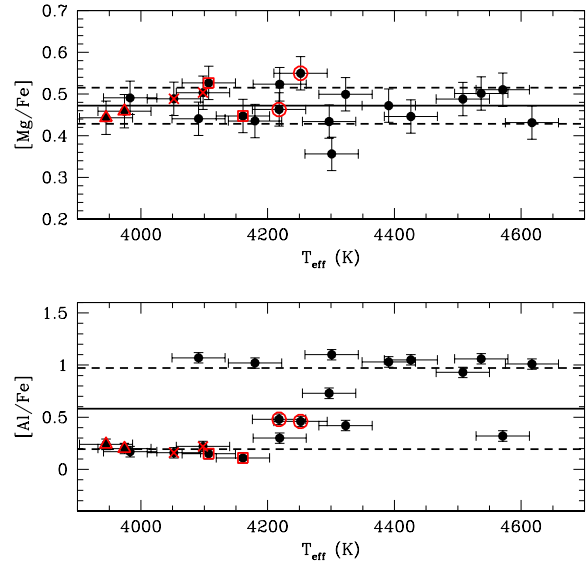


Figure 5. [Mg/Fe] and [Al/Fe] vs. T_{eff} for our targets. The 4 stars observed twice are indicated with 4 different red open symbols.

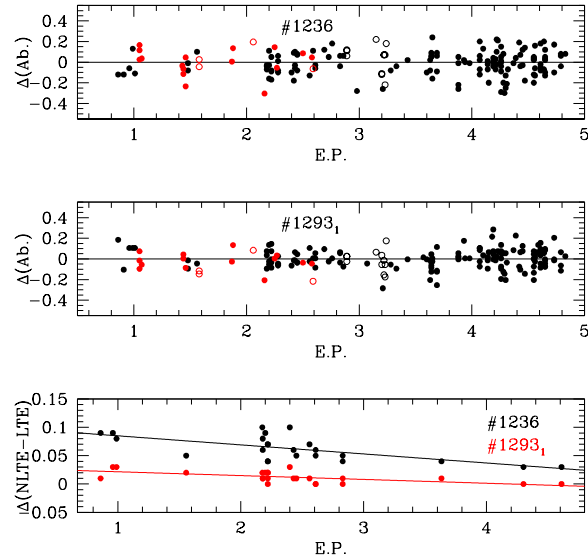


Figure 6. Upper panel: FeI (filled black circles), FeII (open black circles), TiI (filled red circles), and TiII (open red circles) differential abundances for stars #1236. Middle panel: FeI (filled black circles), FeII (open black circles), TiI (filled red circles), and TiII (open red circles) differential abundances for stars #1293₁. Lower panel: NLTE correction as a function of E.P. for iron lines for star #1236 (black points, $T_{\text{eff}}=4617$ K) and #1293₁ (red points, $T_{\text{eff}}\sim 3950$ K). Linear fits are indicated as continuous lines.

While for stars #1293₁ ($T_{\text{eff}}\sim 4000$ K, red points) the NLTE correction is very small along the entire E.P. range and can be neglected, for stars #1236 ($T_{\text{eff}}\sim 4600$ K, black points) reaches ~ 0.1 dex for lines with E.P.=1. For this star we performed again the spectroscopic analysis applying to FeI lines the NLTE correction of Fig. 6 (lower panel, black line). The result was a slight change in the atmospheric param-

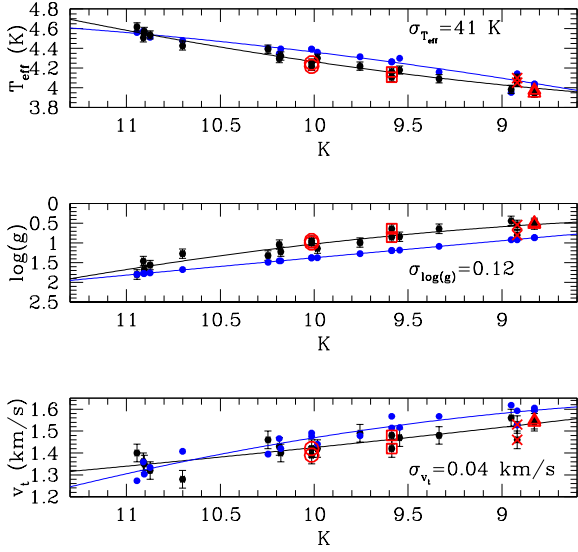


Figure 7. T_{eff} , $\log(g)$, and v_t as a function of K magnitude for our targets. The 4 stars observed twice are indicated with 4 different red open symbols. Temperature values are given divided by 1000.

ters ($T_{\text{eff}}=4565$ K, $\log(g)=1.70$, and $v_t=1.40$ km/s) but a negligible change in metallicity ($[\text{Fe}/\text{H}]_{\text{LTE/NLTE}}=-1.16/-1.17$). This is because NLTE corrections cause a downward change of the temperature that counterbalances the mean $+0.06$ dex correction mentioned before. The conclusion of this test is that NLTE cannot be the reason of the $[\text{Fe}/\text{H}]$ trend.

If we look carefully to the trend however, we notice that stars between $T_{\text{eff}}=4100$ K and $T_{\text{eff}}=4520$ K show a very flat slope that deviates from the 0 value of less than 0.2σ . So the $[\text{Fe}/\text{H}]$ trend is entirely due to the three warmer and to the three cooler points, that deviate from the mean iron abundance of $\sim 1.5 \sigma$ and $\sim 1.0 \sigma$ respectively. Actually Fig. 2 shows that 5 out of 21 points deviate of 1σ or more with respect to the mean $[\text{Fe}/\text{H}]$ abundance, that represents 24% of the sample. This matches very well with deviation that is expected statistically, because 22% of the points are expected to fall out of the $\sim 1\sigma$ range. Because of this there is no reason not to attribute the $[\text{Fe}/\text{H}]$ trend to statistical fluctuations. This is supported also by the error analysis (see Tab. 4 and below) that gives an expected r.m.s for our data of 0.06 dex that matches very well the observed spread of 0.06 dex. Maybe some other mechanism is at work like molecular bands that could affect the position of the continuum for the two cooler stars (in this case the continuum would be depressed causing an underestimation of the EQWs and so lower abundances for iron but also for all the other elements), but the accuracy of our measurements is not high enough to disentangle such a mechanism from statistical noise.

As far as Silicon, Calcium, Nickel, and Barium abundance ratios are concerned all stars are spread around the mean value and no sign of trend is present. Only Ti appears to have a slight trend with temperature but the range in $[\text{Ti}/\text{Fe}]$ of our data is so small (~ 0.1 dex) that it is hard to

attribute this to a cause other than statistical fluctuation, at least with the current internal accuracy of our measurements. However, since Ti final abundance was obtained from neutral and single ionized lines, we plotted in Fig. 6 (upper and middle panels) the differential Ti and TiII abundances. As in the case of FeI and FeII, TiI lines follow a flat trend while TiII lines are spread around the mean TiII abundance. TiI and TiII are sensitive to stellar parameters but were not used to obtain them. For this reason this check shows that the method we used to obtain T_{eff} and $\log(g)$ is robust.

As a final conclusion we can say that the methodology used to obtain chemical abundances is consistent over the entire temperature range with possible minor trends on $[\text{Fe}/\text{H}]$ and $[\text{Ti}/\text{Fe}]$ with effective temperature that anyway could be due to statistical fluctuations and do not affect the results.

Fig. 4 and Fig. 5 show the light elements O, Na, Mg, and Al abundances vs. T_{eff} . Those are the most important elements for the following discussion. We see that O, Na, Mg, and Al do not show any trend with T_{eff} and the large spread around the mean value is due to the presence in the cluster of stars with inhomogeneous abundances.

A detailed internal error analysis was performed using two methods. For the first we plotted in Fig. 7 temperature, gravity and microturbulence of our stars as a function of the $K_{2\text{MASS}}$ magnitude (black points). Because the error on $K_{2\text{MASS}}$ is negligible in this plot (0.01–0.02 mag.), the dispersion around the parabolic fit (black lines) is entirely due to errors on the atmospheric parameters. This dispersion gives us $\sigma(T_{\text{eff}})=41$ K, $\sigma(\log(g))=0.12$, and $\sigma(v_t)=0.04$ km/s. The error on $[\text{Fe}/\text{H}]$ due to the S/N is 0.01 dex. As a comparison, in Fig. 7 we plotted with blue points our initial guess for temperature, gravity, and microturbulence as obtained from photometry together with a parabolic fit (blue lines). As far as T_{eff} is concerned, for warmer and cooler targets the match is reasonably good while in the middle region photometric temperatures are about 100–150 K higher. The mean difference is about 60 K. We underline the fact that if we would have adopted photometric temperature, targets in the middle region would have had a $[\text{Fe}/\text{H}]$ value 0.15–0.20 dex larger than the others, while with the temperature scale we adopt in this paper the $[\text{Fe}/\text{H}]$ value of all the stars agree well within the errors (see Tab. 4). On the other hand our gravities are 0.3 dex lower on average than the photometric values while microturbulences are 0.05 km/s lower, with the warmer stars showing a better agreement. These mismatches could be due to the poorly known parameters of the cluster (a change in distance modulus of $+0.1$ mag and in the reddening of -0.05 mag would give an almost negligible difference in temperature and an agreement within 0.2 dex in gravity) or to effects not taken into account by the models (i.e. 3D effects).

The second method is based on the 4 stars observed twice (#1246, #1293, #1378, and #1380). We derived the atmospheric parameters independently from the individual spectra of each star. Then we computed the differences in T_{eff} , $\log(g)$ and v_t , between the two determinations. The distribution of atmospheric parameters differences gives us $\sigma(T_{\text{eff}})=33$ K, $\sigma(\log(g))=0.12$, and $\sigma(v_t)=0.03$ km/s and a total error on $[\text{Fe}/\text{H}]$ of 0.03 dex. This total error takes into account all the errors on the atmospheric parameters.

The two methods agree well, and we adopted $\sigma(T_{\text{eff}})=40$

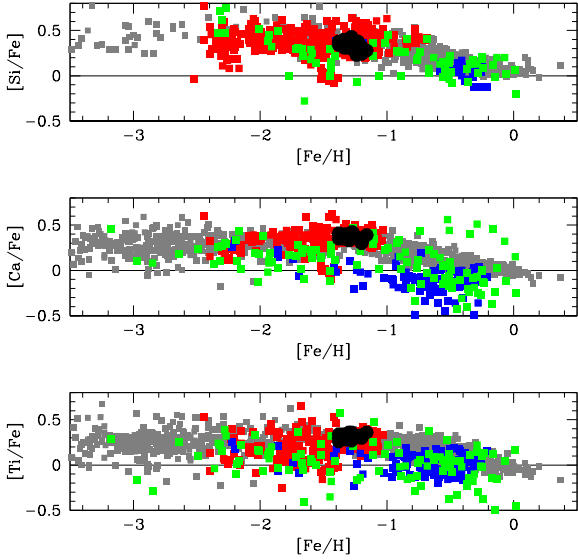


Figure 8. Star by star (black filled circles) abundances for M28 compared with a variety of Galactic and extragalactic environments: Galactic Globular Clusters (red filled squares); Disc and Halo stars (gray filled squares); Magellanic clouds (blue filled squares); other dwarf and ultra-faint dwarf galaxies (Draco, Sextans, Ursa Minor, Sagittarius, Boötes I and Hercules, green filled squares). See text for more details.

K, $\sigma(\log(g))=0.12$, $\sigma(v_t)=0.04$, and $\sigma([Fe/H])=0.03$ dex as our final errors on the atmospheric parameters. Then we choose star #1367 as representative of the sample, varied its T_{eff} , $\log(g)$, $[Fe/H]$, and v_t according to the atmospheric errors we just obtained, and redetermining the abundances. Results are shown in Tab. 4, including the error due to the noise of the spectra. This error was obtained for elements whose abundance was obtained by EQWs, as the errors on the mean given by MOOG, and for elements whose abundance was obtained by spectrum-synthesis, as the error given by the fitting procedure. Δ_{tot} is the squared sum of the single errors, while $\Delta_{\text{tot}}(\text{obs})$ is the error as obtained from the 4 repeated stars. $\Delta_{\text{tot}}(\text{obs})$ is equal or smaller than Δ_{tot} . In Tab. 4 for each element we report the observed spread of the sample (RMS_{obs}) with its error and in the final column the significance (in units of σ) calculated as the absolute value of the difference between RMS_{obs} and Δ_{tot} divided by the error on RMS_{obs} (we choose Δ_{tot} instead of $\Delta_{\text{tot}}(\text{obs})$ to be conservative). This tells us if the observed dispersion RMS_{obs} is intrinsic or due to observational errors. Values larger than 3σ imply an intrinsic dispersion in the species chemical abundance among the cluster stars.

4 RESULTS

4.1 Iron-peak, α elements and heavy elements

The mean iron content we obtained is:

$$[Fe/H] = -1.29 \pm 0.01$$

with a dispersion of:

$$\sigma_{[Fe/H]} = 0.06 \pm 0.01$$

Reported errors are errors on the mean. Harris (1996) gives $[Fe/H]=-1.32$ and we can consider the agreement satisfactory. The measured iron dispersion in Tab. 4 well agrees with the dispersion due to measurement errors so we no evidence for an intrinsic Fe abundance spread. As far as iron-peak elements are concerned, Cr and Ni are solar scaled, Mn and Cu are sub-solar, and V, Co and Zn are super-solar.

The α elements Si, Ca, and Ti are overabundant compared to the Sun. This is a feature common to almost all Galactic GC and Halo field stars as well as to very metal-poor stars ($[Fe/H]<-1.5$) in outer galaxies. Based on these elements we derive for the cluster a mean α element abundance of:

$$[\alpha/Fe] = +0.34 \pm 0.01$$

As far as heavy elements are concerned Y, Zr, Ba, and Eu are super-solar, La is solar-scaled and Ce is sub-solar.

Figure 8 shows the star by star (black filled circles) α -element abundances of the cluster compared with a variety of galactic and extra-galactic objects. We have included values from Galactic Globular Clusters (GCs) (Carretta et al. 2009b, 2010, 2014a,b, 2015a,b; Villanova et al. 2010, 2011, 2013; Muñoz et al. 2013; San Roman et al. 2006, red filled squares); Disc and Halo stars (Fulbright 2000; Reddy et al. 2003, 2006; Cayrel et al. 2004; Simmerer 2004; Barklem et al. 2005; Francois et al. 2007; Johnson et al. 2012, 2014, gray filled squares) and extra-galactic objects such as Magellanic clouds (Pompeia et al. 2008; Johnson et al. 2006; Mucciarelli et al. 2008, 2009, blue filled squares), Draco, Sextans, Ursa Minor and Sagittarius dwarf galaxy and the ultra-faint dwarf spheroidals Boötes I and Hercules (Monaco et al. 2005; Sbordone et al. 2007; Shetrone et al. 2001; Ishigaki et al. 2014; Koch et al. 2008, green filled squares).

The α elements in M28 follows the same trend as Galactic GCs and are fully compatible with Halo field stars while it falls in a region scarcely populated by extragalactic objects. So, according to its α -element content, M28 is very likely a genuine Galactic cluster.

The chemical abundances for the iron-peak elements Mn and Cu are reported in Fig. 9. Around M28 metallicity, Galactic and extragalactic environments share the same Mn abundance, while the cluster Cu content agrees better with the Galaxy. This further supports a Galactic origin.

Finally for all α , iron-peak and heavy elements Tab. 4 shows that the observed dispersion agrees well with the measurement errors so we can rule out any intrinsic abundance spread. We check also for possible correlations of these elements with light elements such Na and Al, but we did not find evidence for significant trends.

4.2 Light elements

Light elements O, Na, and Al have an observed spread that well exceeds the observational uncertainties (see Tab. 4). The only exception is Mg that seems to be homogeneous within the errors.

In Fig. 10 and Fig. 11 we compare the O and Al abun-

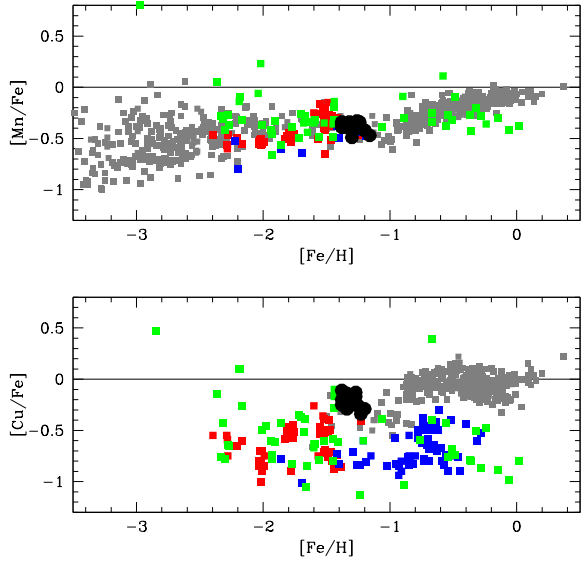


Figure 9. Star by star (black filled circles) abundances for M28 compared with a variety of Galactic and extragalactic environments: Galactic Globular Clusters (red filled squares); Disc and Halo stars (gray filled squares); Magellanic clouds (blue filled squares); other dwarf and ultra-faint dwarf galaxies (Draco, Sextans, Ursa Minor, Sagittarius, Bootes I and Hercules, green filled squares). See text for more details.

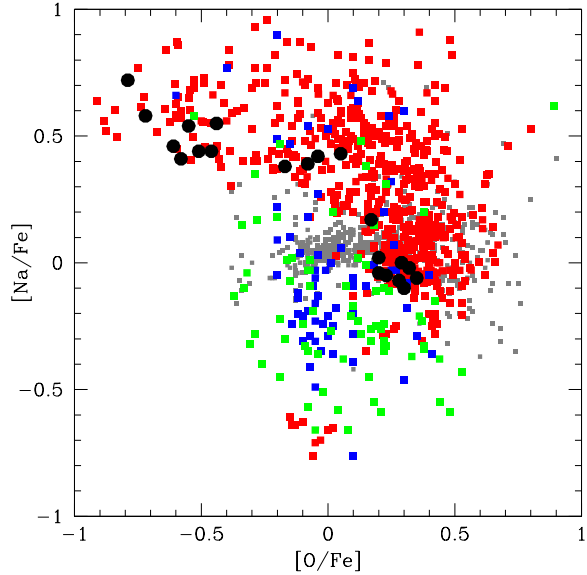


Figure 11. Na-O anticorrelation for M28 (black filled circles) compared with a variety of Galactic and extragalactic environments: Galactic Globular Clusters (red filled squares); Disc and Halo stars (gray filled squares); Magellanic clouds (blue filled squares); other dwarf and ultra-faint dwarf galaxies (Draco, Sextans, Ursa Minor, Sagittarius, Bootes I and Hercules, green filled squares). See text for more details.

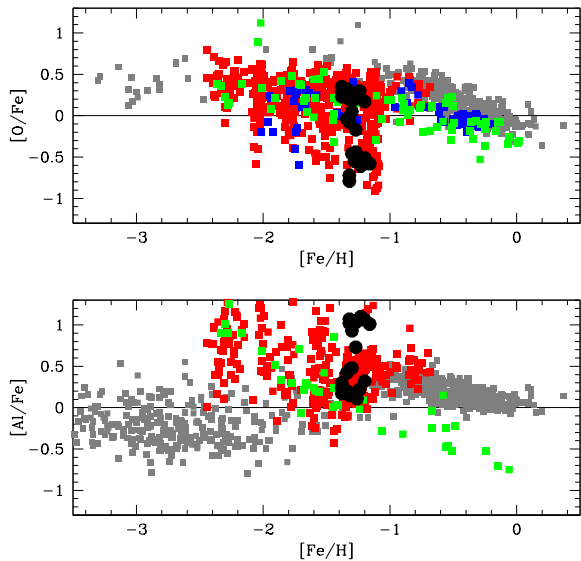


Figure 10. Star by star (black filled circles) abundances for M28 compared with a variety of Galactic and extragalactic environments: Galactic Globular Clusters (red filled squares); Disc and Halo stars (gray filled squares); Magellanic clouds (blue filled squares); other dwarf and ultra-faint dwarf galaxies (Draco, Sextans, Ursa Minor, Sagittarius, Bootes I and Hercules, green filled squares). See text for more details.

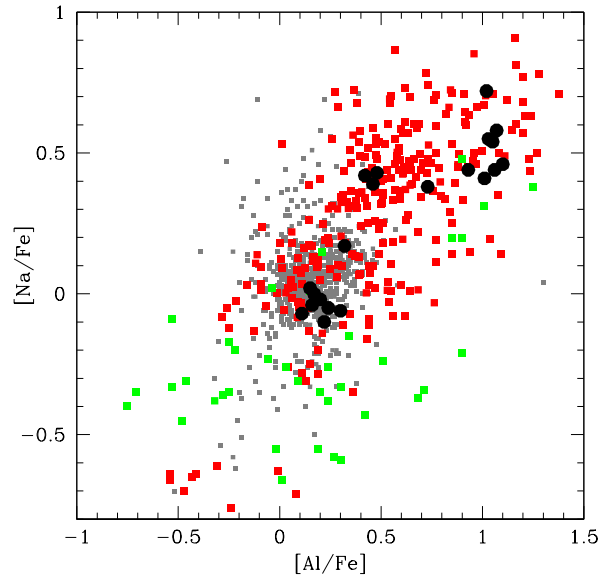


Figure 12. Na-Al correlation for M28 (black filled circles) compared with a variety of Galactic and extragalactic environments: Galactic Globular Clusters (red filled squares); Disc and Halo stars (gray filled squares); Magellanic clouds (blue filled squares); other dwarf and ultra-faint dwarf galaxies (Draco, Sextans, Ursa Minor, Sagittarius, Bootes I and Hercules, green filled squares). See text for more details.

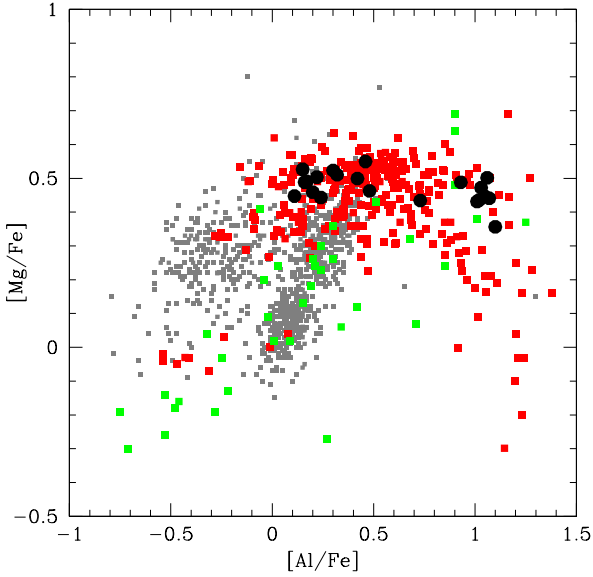


Figure 13. Mg-Al anticorrelation for M28 (black filled circles) compared with a variety of Galactic and extragalactic environments: Galactic Globular Clusters (red filled squares); Disc and Halo stars (gray filled squares); Magellanic clouds (blue filled squares); other dwarf and ultra-faint dwarf galaxies (Draco, Sextans, Ursa Minor, Sagittarius, Bootes I and Hercules, green filled squares). See text for more details.

dances of the targets with different environments. The content of the two elements of the M28 first generation stars (the targets with $[O/Fe] \sim 0.3$, $[Na/Fe] \sim 0.0$, $[Al/Fe] \sim 0.2$) well matches the mean O and Al abundances of the Milky Way Halo and the mean O and Al content of the other GC first generation stars. It matches also the O and Al content of extragalactic environments. On the other hand the cluster shows a strong depletion in O and a strong Al enhancement as far as the subsequent generation targets are concerned (the targets with $[O/Fe] < 0.3$, $[Na/Fe] > 0.1$, $[Al/Fe] > 0.2$). Actually M28 is one of the clusters that shows the strongest O depletion (down to $[O/Fe] \sim -0.8$) and the strongest Al enhancement (up to $[Al/Fe] \sim +1.1$) together with few other GCs in the Milky Way (e.g. NGC 2808, NGC 3201, and NGC 6752) and in the Large Magellanic Cloud (e.g. NGC 1718).

Fig. 11 shows the Na-O anticorrelation for M28. First generation stars have a Na content that is lower than the bulk of Milky Way field objects. The second generation stars follow the Galactic GC trend along the O-poor edge (left edge). This is because M28 has one of the lowest initial O contents ($[O/Fe] \sim 0.3$) with respect to the other GCs. This relatively low O content is maintained when subsequent generations stars are formed. The cluster population ends up with two stars (#1291 and #1295) that are among the most O-poor star in the GC sample we have. This means that M28 suffered one of the most extensive nuclear processing. Fig. 11 shows also the star formation process was not continuous, but it happened with different bursts because our targets aggregate in at least three different clumps.

Fig. 12 and Fig. 13 show the Na-Al and Mg-Al correlations. The cluster follows the typical correlations of the GCs, with

Al-rich stars ($[Al/Fe] > 0.8$) that appear to be slightly Mg-poorer than the others on average. However the most surprising result is that in the Na-Al correlation stars appear to be clearly aggregated in 3 clumps and that the abundance evolution is not linear.

In order to investigate in more detail this behavior we plot in Fig. 14 light-element correlations or anticorrelations. Errorbars are from Table 4 (7th column). We analyze this figure starting from the Na-Al plot (upper right panel). As said before, it is clear that stars do not follow a linear trend (the continuous thin line) but very likely a *segmented* path that we indicated with a continuous thick line. Stars below $[Al/Fe] = 0.5$ increment their Na and Al content linearly. After that stars appear to have a constant Na content ($[Na/Fe] \sim 0.4$) while Al increase up to $[Al/Fe] \sim +1.0$. Finally stars evolve to higher Na abundances (up to $[Na/Fe] \sim 0.7$) maintaining Al constant. In order to support this statement we calculated the distance of the points from the linear trend. If we decompose this distance into a vector along the X axis, that corresponds to the deviation of the $[Al/Fe]$ abundance of the point, and into a vector along the Y axis, that corresponds to the deviation of the $[Na/Fe]$ abundance of the point, we obtain the deviations of the $[Na/Fe]$ and $[Al/Fe]$ abundances of our data with respect to the linear trend. The r.m.s of these deviations would imply an error on our $[Na/Fe]$ values of 0.09 ± 0.01 dex and an error on our $[Al/Fe]$ values of 0.06 ± 0.01 dex. If we assume that the error on $\Delta_{tot}(Na)$ is also 0.01 as Tab. 4 suggests, we find that the value for $[Na/Fe]$ exceeds more than 3σ the error estimation of Tab. 4 according to the equation:

$$Significance = (0.09 - 0.04) / (\sqrt{(0.01^2 + 0.01^2)}) \sigma = 3.5 \sigma$$

and that for $[Al/Fe]$ is larger too. So we conclude that a linear trend is a very poor approximation of the data.

In this evolutionary path our targets are not distributed uniformly but aggregate in clumps. There are at least 3 of them at 1) $[Al/Fe] \sim 0.2$, $[Na/Fe] \sim -0.1$ (blue points), $[Al/Fe] \sim 0.4$, $[Na/Fe] \sim 0.4$ (red points), and 3) $[Al/Fe] \sim 1.0$, $[Na/Fe] \sim 0.5$ (green points) with some interlooper. The third group has a spread much larger than the other two (up to 0.2 dex), and could be composed of two further sub-populations. However more data are required to constrain better the number of sub-populations in M28. We underline the fact that it is not unusual for a GC to show discrete sub-populations. As an example Milone et al. (2015) found that NGC 2808 is formed by 5 or more discrete sub-populations.

In the upper left panel of Fig. 14 we report the Na-O anticorrelation. We fitted the Carretta et al. (2009a) dilution model (dashed black line). According to this fit the cluster is composed by a first generation of stars with $[Na/Fe] \sim -0.10$ and $[O/Fe] \sim +0.30$ and subsequent generations ends up with $[Na/Fe] \sim +0.55$ and $[O/Fe] \sim -0.6$. However, while this model fits well the blue and red sub-populations, it fails for the green. In particular the most O-poor stars show a spread in Na that is not reproduced at all by the dilution model. Based in what we have found above, we fitted a segmented anticorrelation represented by the continuous black line. Stars above $[O/Fe] = -0.3$ increment their Na and decrement they O contents linearly. After that stars appear to have a constant Na content ($[Na/Fe] \sim 0.4$) while O decreases down to $[O/Fe] \sim -0.5$. Finally stars evolve to higher Na abun-

dances (up to $[\text{Na}/\text{Fe}] \sim 0.7$) and lower O abundances (down to $[\text{O}/\text{Fe}] \sim -0.7$) linearly.

In the lower panel on the left we report the Al-O anticorrelation. At odd with the previous plots, the anticorrelation is linear down to $[\text{O}/\text{Fe}] \sim -0.5$ with aluminum that increases while oxygen decreases. After that the correlation seems to twist with very O-poor stars that decrease their aluminum content.

Finally in the lower panel on the right we plot $[\text{Mg}/\text{Fe}]$ vs. $[\text{Al}/\text{Fe}]$. The error analysis did not show evidence for a intrinsic spread of Mg for our stars. On the other end here we see that Al-rich stars are also Mg-poor and the trend has a slope with a significance at the level of 3σ . This is not unexpected since aluminum is produced by the Mg-Al chain at the expenses of Mg (Ventura et al. 2011) in intermediate-mass AGB stars, that are one of the main candidates responsible for the multiple-population phenomenon and that are the only candidates able to activate this chain since they reach high enough temperatures (~ 75 million K) during the hot-bottom-burning phase (D’Antona et al. 2016).

5 SUMMARY

In this paper we present the first detailed chemical abundances of 21 elements in 17 red giant radial velocity and metallicity members of M28 observed using the high resolution UVES spectrograph, mounted at the VLT-UT2 telescope. M28 is a metal poor GC ($[\text{Fe}/\text{H}] \sim -1.3$) and must be very old (~ 13 Gyrs) because of the HB morphology that completely lacks a red branch. Chemical abundances have been computed using plane-parallel atmospheric-models and LTE approximation. Equivalent width method has been used when possible. Otherwise we applied the spectrum-synthesis method. We obtained the following results:

- We found a mean metallicity of $[\text{Fe}/\text{H}] = -1.29 \pm 0.01$, that well agree with previous literature data. As far as other iron-peak elements are concerned, Cr and Ni are solar-scaled, Mn and Cu are sub-solar, and V, Co, and Zn are super-solar.

- M28 has the typical α -enhancement of the Halo with $[\alpha/\text{Fe}] = +0.34 \pm 0.01$. Heavy elements Y, Zr, Ba, and Eu are super-solar, La is solar scaled and Ce is sub-solar. We did not find any intrinsic spread in any of these elements, and no correlation with light elements.

- M28 shows the typical Na-O anticorrelation common to almost all the other GCs. The cluster also show a Na-Al correlation and a Mg-Al anticorrelation. It is one of the clusters that shows the strongest O depletion and Na and Al enhancement among all the GCs studied up to now. The presence of a Mg-Al anticorrelation points toward intermediate-mass AGB stars as the main polluters responsible for the multiple-population phenomenon in this cluster.

- The most interesting results however concerns the shape and discreteness of the Na-Al and Na-O relations. Both appears to be not linear or parabolic, but *segmented*, and stars are not distributed continuously, but seems to form at least 3 different sub-populations. This is not totally new since also the GC NGC 2808 shows the presence of at least 5 distinct sub-populations. A larger sample of data is required to confirm if more sub-populations are present.

ACKNOWLEDGMENTS

SV and CMB acknowledge the support provided by Fondecyt Regular 1130721 and 1150060, respectively. FM gratefully acknowledges the support provided by Fondecyt for project 3140177. LM acknowledges support from “*Proyecto Interno*” of the Universidad Andres Bello.

REFERENCES

- Alonso, A., Arribas, S., & Martinez-Roger, C. 1999, *A&AS*, 140, 261
- Barklem, P. S., Christlieb, N., Beers, T. C., Hill, V., Bessell, M. S., Holmberg, J., Marsteller, B., Rossi, S., Zickgraf, F. J., & Reimers, D. 2005, *A&A*, 439, 129
- Bastian, N., Lamers, H. J. G. L. M., de Mink, S. E., Longmore, S. N., Goodwin, S. P., & Gieles, M. 2013, *MNRAS*, 436, 2398
- Bica, E., Ortolani, S., & Barbuy, B. 2015arXiv151007834B
- Caloi, V., & D’Antona, F. 2011, *MNRAS*, 417, 228
- Carretta, E., Bragaglia, A., Gratton, R.G., Lucatello, S., Catanzaro, G., Leone, F., Bellazzini, M., Claudi, R., D’Orazi, V., Momany, Y., Ortolani, S., Pancino, E., Piotto, G., Recio-Blanco, A., & Sabbi, E. 2009, *A&A*, 505, 117
- Carretta, E., Bragaglia, A., Gratton, R.G., Lucatello, S., Catanzaro, G., Leone, F., Bellazzini, M., Claudi, R., D’Orazi, V., & Momany, Y. 2009, *A&A*, 505, 139
- Carretta, E., Bragaglia, A., Gratton, R. G., Lucatello, S., Bellazzini, M., Catanzaro, G., Leone, F., Momany, Y., Piotto, G. & D’Orazi, V. 2010, *A&A*, 520, 95
- Carretta, E., Bragaglia, A., Gratton, R. G., D’Orazi, V., Lucatello, S., Momany, Y.,
- Carretta, E., Bragaglia, A., Gratton, R. G., D’Orazi, V., Lucatello, S., & Sollima, A. 2014, *A&A*, 561, 87
- Carretta, E., Bragaglia, A., Gratton, R. G., D’Orazi, V., Lucatello, S., Sollima, A., Momany, Y., Catanzaro, G., & Leone, F. 2015, *A&A*, 578, 116
- Carretta, E. 2015, *ApJ*, 810, 148
- Cayrel, R., Depagne, E., Spite, M., Hill, V., Spite, F., Francois, P., Plez, B., Beers, T., Primas, F., Andersen, J. et al. 2004, *A&A*, 416, 1117
- Chené, A. N., Borissova, J., Clarke, J. R. A., et al. 2012, *A&A*, 545, A54
- Cohen, J. G., Kirby, E. N., Simon, J. D., & Geha, M. 2010, *ApJ*, 725, 288
- D’Antona, F., Vesperini, E., D’Ercole, A., Ventura, P., Milone, A. P., Marino, A. F., & Tailo, M. 2016, *MNRAS*, 458, 2122
- Davidge, T. J., Cote, Patrick, & Harris, W. E. 1996, *ApJ*, 468, 641
- de Mink, S. E., Pols, O. R., Langer, N., & Izzard, R. G. 2009, *A&A*, 507, 1
- Decressin, T., Meynet, G., Charbonnel, C., Prantzos, N., & Ekstrom, S. 2007, *A&A*, 464, 1029
- D’Orazi, V., Angelou, G.C., Gratton, R. G., Lattanzio, J. C., Bragaglia, A., Carretta, E., Lucatello, S., & Momany, Y. 2014, *ApJ*, 791, 39
- Gray, R. O. & Corbally, C. J. 1994, *AJ*, 107, 742
- Fulbright, J. P. 2000, *AJ*, 120, 1841
- Francois, P., Depagne, E., Hill, V., Spite, M., Spite, F.,

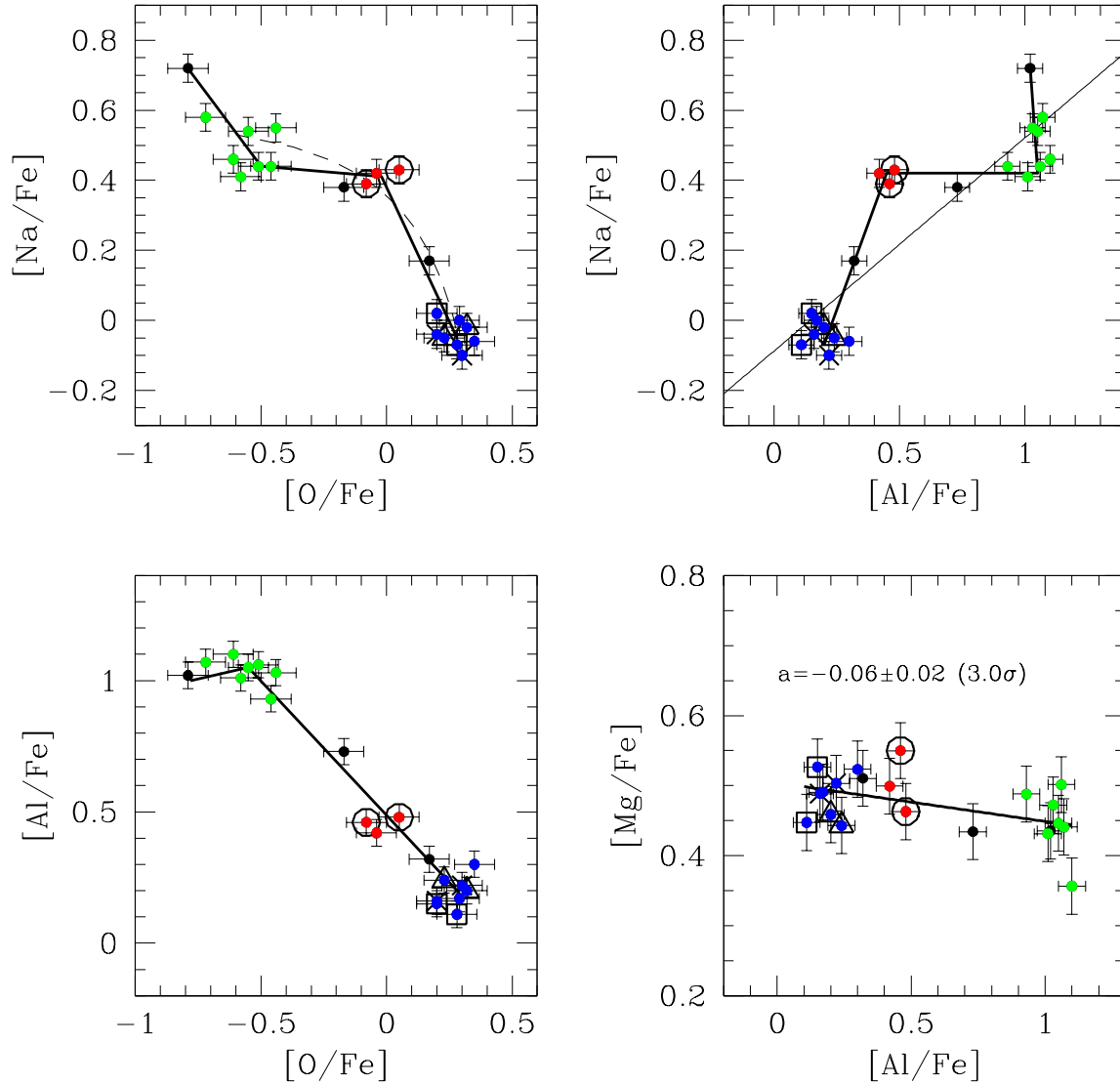


Figure 14. Na-O anticorrelation (upper left panel), Na-Al correlation (upper right panel), Al-O anticorrelation (lower left panel), and Mg-Al anticorrelation (lower right panel) for M28. The 4 stars observed twice are indicated with 4 different black open symbols. See text for more details.

Plez, B., Beers, T. C., Andersen, J., James, G., Barbuy, B. et al. 2007, *A&A*, 476, 935
 Harris, W.E. 1996, *AJ*, 112, 1487
 Ishigaki, M. N., Aoki, W., Arimoto, N., & Okamoto, S. 2014, *A&A*, 562, 146
 Johnson, J. A., Ivans, I. I., & Stetson, P. B. 2006, *ApJ*, 640, 801
 Johnson, C. I., Rich, R. M., Kobayashi, C., & Fulbright, J. P. 2012, *ApJ*, 749, 175
 Johnson, C. I., Rich, R. M., Kobayashi, C., Kunder, A., & Koch, A. 2014, *AJ*, 148, 67
 Koch, A., McWilliam, A., Grebel, E. K., Zucker, D. B., & Belokurov, V. 2008, *ApJ*, 688, 13
 Kurucz, R.L. 1970, *SAO Special Report*, 309
 Larsen, S. S., Brodie, J. P., & Strader, J. 2012, *A&A*, 546,

53

Letarte, B., Hill, V., Jablonka, P., Tolstoy, E., Francois, P., & Meylan, G. 2006, *A&A*, 453, 547
 Marino, A.F., Villanova, S., Piotto, G., Milone, A.P., Momany, Y., Bedin, L.R. & Medling, A.M. 2008, *A&A*, 490, 625
 Marino, A.F., Milone, A.P., Piotto, G., Villanova, S., Bedin, L.R., Bellini, A., & Renzini, A. 2009, *A&A*, 505, 1099
 Mauro, F., Moni Bidin, C., Chene, A. N., et al. 2013, *Revista Mexicana de Astronomía y Astrofísica*, 49, 189
 Massari, D., Mucciarelli, A., Ferraro, F. R., Origlia, L., Rich, R. M., Lanzoni, B., Dalessandro, E., Valenti, E., Ibata, R., Lovisi, L., et al. 2014, *ApJ*, 795, 22
 A. P. Milone, A. F. Marino, G. Piotto, A. Renzini, L. R. Bedin, J. Anderson, S. Cassisi, F. D'Antona, A. Bellini,

- H. Jerjen, A. Pietrinferni, & P. Ventura ApJ, 808, 1
Minniti, D., Lucas, P. W., Emerson, J. P., et al. 2010, New Astronomy, 15, 433
Moni Bidin, C., Mauro, F., Geisler, D., et al. 2011, A&A, 535, A33
Mucciarelli, A., Carretta, E., Origlia, L., & Ferraro, F. R. 2008, AJ, 136, 375
Mucciarelli, A., Origlia, L., Ferraro, F. R., & Pancino, E. 2009, ApJ, 695, 134
Mucciarelli, A., Dalessandro, E., Ferraro, F. R., Origlia, L., & Lanzoni, B. 2014, ApJ, 793, 6
Muñoz, C., Geisler, D., & Villanova, S. 2013, MNRAS, 433, 2006
Monaco, L., Bellazzini, M., Bonifacio, P., Ferraro, F. R., Marconi, G., Pancino, E., Sbordone, L., & Zaggia, S. 2005, A&A, 441, 141
Pompeia, L., Hill, V., Spite, M., Cole, A., Primas, F., Romaniello, M., Pasquini, L., Cioni, M.R., & Smecker Hane, T. 2008, A&A, 480, 379
Ramirez, I., & Melendez, J. 2005, ApJ, 626, 446
Reddy, B. E., Tomkin, J., Lambert, D. L., & Allende Prieto, C. 2003, MNRAS, 340, 304
Reddy, B. E., Lambert, D. L., & Allende Prieto, C. 2006, MNRAS, 367, 1329
Saito, R. K., Hempel, M., Minniti, D., et al. 2012, A&A, 537, A107
San Roman, I., Munoz, C., Geisler, D., Villanova, S., Kacharov, N., Koch, A., Carraro, G., Tautvaisiene, G., Vallenari, A., Alfaro, E. J. et al. 2015, A&A, 579, 6
Sbordone, L., Bonifacio, P., Buonanno, R., Marconi, G., Monaco, L., Zaggia, S. 2007, A&A, 465, 815
Shetrone, M. D., Cote, P., Sargent, W. L. W. 2001, ApJ, 548, 592
Simmmerer J. 2004, AAS, 205, 7705
Skrutskie, M. F., Cutri, R. M., Stiening, R., et al. 2006, AJ, 131, 1163
Snedden, C. 1973, ApJ, 184, 839
Stetson, P. B., & Pancino, E. 2008, PASP, 120, 1332
VandenBerg, D. A., Brogaard, K., Leaman, R., & Casagrande, L. 2013, ApJ, 775, 134
Ventura, P., Carini, R., & D'Antona, F., 2011, MNRAS, 415, 3865
Villanova, S., Geisler, D., & Piotto, G. 2010, ApJ, 722, 18
Villanova, S., & Geisler, D. 2011, A&A, 535, 31
Villanova, S., Geisler, D., Carraro, G., Moni Bidin, & C., Muñoz, 2013, ApJ, 778, 186
Villanova, S., Geisler, D., Gratton, R. G., & Cassisi, S. 2014, ApJ, 791, 107

This paper has been typeset from a \TeX / \LaTeX file prepared by the author.